PHYSICAL REVIEW E VOLUME 62, NUMBER 5 NOVEMBER 2000

Direct observation of a twist mode in electroconvection

Michael Dennin
Department of Physics and Astronomy, University of California at Irvine, Irvine, California 92697-4575

(Received 31 March 2000)

I report on the direct observation of a uniform twist mode of the director field in electroconvection in the nematic liquid crystal I52. Recent theoretical work suggests that such a uniform twist mode of the director field is responsible for a number of secondary bifurcations in both electroconvection and thermal convection in nematics. I show here evidence that the proposed mechanisms are consistent with being the source of the previously reported stationary oblique roll pattern identified as the SO2 state of electroconvection in the liquid crystal I52. The same mechanisms also contribute to a tertiary Hopf bifurcation that I observe in electroconvection in the liquid crystal I52. There are quantitative differences between the experiment and calculations that only include the twist mode. These differences suggest that a complete description must include effects described by the weak-electrolyte model of electroconvection.

PACS number(s): 61.30.−v, 47.54.+r, 47.20.−k, 83.70.Jr

I. INTRODUCTION

When a spatially extended system is driven far from equilibrium, a series of transitions occurs as a function of the external driving force, or control parameter. The initial transition is typically from a spatially uniform state to a state with periodic spatial variations, called a pattern [1]. One can distinguish two general classes of pattern forming systems: isotropic and anisotropic. In isotropic systems, because there is no intrinsic direction in the system, the initial wave vector of the pattern can have any orientation. For anisotropic systems, the uniform state of the system has a special axis and there are at most two degenerate initial wave vectors for the pattern. Electroconvection in nematic liquid crystals has become a paradigm for the study of pattern formation in anisotropic systems [2,3].

Nematic liquid crystals are fluids in which the molecules possess orientational order [4]. The axis along which the molecules are aligned on average is referred to as the director. For electroconvection, a nematic liquid crystal is placed between two glass plates. The plates are treated so that there is a uniform alignment of the director parallel to the plates, i.e., planar alignment. The plates are also coated with a transparent conductor, and the liquid crystal is doped with an ionic impurity. An ac voltage is applied perpendicular to the director. Above a critical value V_c for the voltage, a pattern develops that consists of a periodic variation of the director and charge density with a corresponding convective flow of the fluid. Many of the interesting patterns in electroconvection are the result of *oblique rolls*. Oblique rolls refer to patterns where the wave vector forms a nonzero angle θ with respect to the initial alignment of the director. Because the director only defines an axis, for each value of θ and wave number q, there are two degenerate states corresponding to wave vectors at the angles θ and $-\theta$. These states are referred to as zig and zag, respectively.

Electroconvection has been extensively studied experimentally [3]. However, despite a relatively early identification of the basic instability mechanism [5,6], a detailed, quantitative description of the rich array of patterns has only recently emerged. The first step in this development was the elucidation of the standard model of electroconvection [7,8]. The linear stability analysis and weakly nonlinear analysis presented in Ref. [7] accurately describes electroconvection at relatively high electrical conductivities and thick samples. However, it fails to account for traveling patterns, i.e., a Hopf bifurcation, that are observed in thin samples and at low sample conductivity [9,10]. Also, the original weakly nonlinear analysis of the standard model does not explain the experimentally observed ‘‘abnormal’’ rolls [11,12]. Recently, these two phenomena have been explained by independent theoretical extensions of the standard model that are described below.

First, the weak-electrolyte model (WEM) [13,14] is an extension of the standard model that treats the charge density as a dynamically active field and is able to explain the Hopf bifurcation. Second, within the framework of the standard model, secondary and further bifurcations have been assessed with a fully nonlinear Galerkin calculation [11,15]. In particular, this work helped elucidate the decisive role of a homogeneous in-plane twist of the director in the bifurcation to abnormal rolls [11,12]. The general features of this fully nonlinear calculation can be reproduced by an extended weakly nonlinear analysis. This analysis extends previous treatments of the standard model by including the homogeneous twist as a dynamically active mode [15,16], and I will refer to it as the ‘‘twist-mode model.’’ For certain cases, the twist-mode model even provides a semiquantitative or quantitative description of the dynamics. This analysis applies to both electroconvection and thermal convection in nematics [15].

Currently, a weakly nonlinear theory that includes both the WEM effects and the twist mode remains undeveloped. The appropriate merging of the twist-mode model and the WEM is essential for systems with traveling oblique rolls, where both effects can be important. For example, even though electroconvection in the nematic liquid crystal (NLC) I52 provided the first quantitative confirmation of the WEM at the linear level [14], the patterns in NLC I52 are dominated by oblique rolls [17]. Therefore, the homogeneous in-plane twist is present and may be important at the weakly nonlinear level. The main question is: does this mode need to

©2000 The American Physical Society

be included as an additional active mode in an extended weakly nonlinear analysis, or is the WEM model sufficient? In particular, this question is crucial for two patterns that are observed in NLC I52 where the dynamics depends on the interaction between traveling oblique rolls: spatiotemporal chaos at onset [18] and localized states known as ''worms'' [19]. Currently, qualitative features of these patterns have been reproduced in the context of a weakly nonlinear analysis based on the WEM [20]. However, if the twist-mode is an active mode, it must be included for any quantitative comparison to work.

The results reported here are a first step in determining the relative importance of the in-plane homogeneous twist of the director in electroconvection in NLC I52. For these initial experiments, the contribution of WEM effects were minimized by focusing on relatively high conductivities. This work includes a more detailed and quantitative study of stationary oblique roll pattern identified as the SO2 state that was first reported in Ref. [21]. The SO2 state consists of the superposition of rolls with wave vector **q** with rolls with wave vector **k**. The angle between the wave vectors ranged from 72° to 90°, depending on the parameter values. In this paper, I will refer to the initial oblique roll wave vector as **q** and any subsequent wave vector that grows as a result of a secondary instability as the dual wave vector **k**. Also, wave vectors with a positive angle relative to the undistorted director will be referred to as zig type, and wave vectors with a negative angle with respect to the undistorted director will be referred to as a zag type. In general, because of the twofold degeneracy, the initial wave vector **q** can either be zig type or zag type.

In Ref. [15], it has been proposed that the SO2 state is an example of the bimodal varicose state. I will show that this association is correct. Also, I report on direct measurements of a twist mode of the director field in NLC I52 for the oblique roll states and the SO2 states. These measurements confirm that the director-wave-vector frustration mechanism proposed in Ref. [15] is the source of the bimodal instability that results in the SO2 state. It has been predicted in Ref. [15] that the bimodal state can experience a Hopf bifurcation to a time periodic state. In this state, the amplitudes of the **q**, **k**, and homogeneous twist modes all oscillate in time. This state is referred to as the oscillating bimodal varicose [22]. This state has been observed indirectly in thermal convection [22], where only the oscillations of the **q** and **k** modes were observed. I report on observations of this Hopf bifurcation in electroconvection. In particular, I have directly measured the oscillations of the homogeneous twist mode in addition to the oscillations of the **q** and **k** modes.

The sequence of bifurcations reported here is in perfect agreement with the twist-mode model. Also, the measured angle between the **q** and **k** modes agree with predictions of the twist-mode model. However, the location of the bifurcation to the bimodal varicose and the oscillating bimodal varicose in not quantitatively described by the twist-mode model. This is easily attributed to two facts. First, the material parameters are not completely known. Second, the WEM effects are still present at some level in the experimental system and have not yet been incorporated into the model.

The rest of the paper is organized as follows. Section II describes the experimental details. Section III presents the experimental results, and Sec. IV discusses the comparison between the results and the twist-mode model.

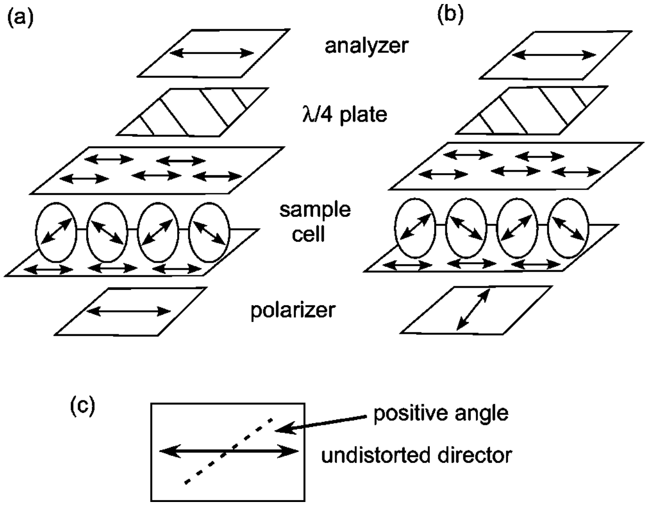

FIG. 1. Schematic drawing of the optical setup. (a) Setup used to image the periodic roll structure. In this case, the polarizer is aligned with the undistorted director axis and extraordinary light is used. (b) Setup used to image the in-plane twist of the director. In this case, the polarizer is rotated 90° with respect to the undistorted director and ordinary light is used. In addition to rotation of the polarizer, both the λ/4 plate and the analyzer are free to rotate. (c) A top view of the cell that shows the undistorted director and the definition of positive angles used for both the in-plane director twist and the orientation of the λ/4 plate. This top view is the same orientation as used for all of the images presented here.

II. EXPERIMENTAL DETAILS

I used the nematic liquid crystal I52 [23] doped with 5% by weight molecular iodine. Commercial cells were obtained from EHC, Ltd. in Japan [24]. The cells consisted of two pieces of glass coated with transparent electrodes of indium-tin oxide (ITO). The surfaces were treated with rubbed polymers to obtain uniform planar alignment. The initial alignment direction will be referred to as the x axis, and the z axis is taken perpendicular to the glass plates. The cell spacing was 23 μm and the electrodes were 1 cm×1 cm. The cells were filled by capillary action and sealed with 5 min epoxy.

The cells were placed in a temperature control block. The temperature was maintained constant to ±2 mK. In order to study a range of parameters, four different operating temperatures were used: 35, 42, 45, and 55 °C.

The system used to image the patterns is shown in Fig. 1. It is a standard shadow graph setup that is modified to allow for the direct observation of in-plane twist modes of the director using a λ/4 plate and analyzer. Two main orientations of the polarizer, λ/4 plate, and analyzer were used. In Fig. 1(a), the polarizer and analyzer are shown parallel to each other and the initial alignment of the director. With this geometry, only the transmission of extraordinary light is observed. Minus the λ/4 plate and analyzer, this is the standard shadow graph setup for electroconvection. The light is focused by the director variation in the x-z plane, and an image of the pattern is obtained [25]. In the arrangement shown in Fig. 1(b), the polarizer is oriented perpendicular to the initial alignment of the director. In this case, only ordinary incident light is present, and the contrast due to the x-z periodic variation is avoided.

In both cases, the $\lambda/4$ plate at 45° to the undistorted director orientation is used to discriminate domains of positive and negative x-y director twist. Figure 1(c) is a top view of the cell and illustrates the definition of positive and negative rotation. The optical setup used here is analyzed in detail in Ref. [26] for a thicker cell and different liquid crystal. However, the qualitative features hold true in this case. For the orientations shown in Fig. 1(b), regions of negative twist have an enhanced transmission of light relative to regions of positive twist. Rotating the $\lambda/4$ plate to $-45°$ yields equivalent information, but with complementary intensities. With the polarizer aligned parallel to the undistorted director, the dominant feature of the image is the focusing due to the periodic x-z variation of the director. However, because we also used the $\lambda/4$ plate in this case, there is a modification of the overall intensity when a homogeneous twist is present. In this orientation, because the polarizer and analyzer are both aligned with the undistorted director, a positive twist of the director has an enhanced transmission of light relative to a negative twist of the director when the $\lambda/4$ plate is at $+45°$. Therefore, in both setups, the sign of the twist amplitude can be determined. In the future, a detailed calculation along the lines presented in Ref. [26] is required for quantitative measurements of the twist amplitude.

The images were taken using a standard CCD camera and digitized with an 8-bit framegrabber. All of the images have both a background subtraction and background division performed. The background subtraction was done to remove the effective mean from the image that is due to the fact that the camera digitized images on a 0 to 255 scale. This was necessary to enable detection of the uniform twist mode by Fourier techniques. The presence of a uniform twist shifts the mean intensity of the image and shows up as changes in the amplitude of the zero wave vector. Without the subtraction step, the zero wave vector peak is dominated by the mean caused by the digitizing process.

The electrical conductivity of the sample ranged between 1×10^{-8} and $1\times10^{-9}\ \Omega^{-1}\,\mathrm{m}^{-1}$. The variation in conductivity was due to two effects: the conductivity is temperature dependent and the conductivity decreased slowly in time. At a fixed temperature, the main effect of the conductivity drift is to shift the critical voltage V_c for the onset of convection. The different temperatures were used to study the effect of varying the material parameters and to offset the long term shifts in V_c. By changing the temperature, V_c was kept at $\approx 11V_{\mathrm{rms}}$. For all of the experiments reported here, the drive frequency was 25 Hz.

Because of the shift in V_c, the following protocols were followed for all of the experimental runs. All transitions are reported in terms of $\epsilon=(V/V_c)^2-1$. To determine the various transition points, the voltage was increased in steps of $\Delta\epsilon$ ranging from 0.005 to 0.01 depending on the precision of interest for a given run. For measurements of the onset of the bimodal varicose instability (ϵ_{BV}), a single image was taken after the system was allowed to equilibrate for 10 min. The relevant time scale is the director relaxation time, which for this system is on the order of 0.2 s. As ϵ is increased above ϵ_{BV}, there is a Hopf bifurcation to the oscillating bimodal varicose state at $\epsilon\equiv\epsilon_H$. The value of ϵ_H was determined by quasistatically stepping ϵ from the bimodal varicose state. At each step in ϵ, a time series of images was taken. The power spectrum of the time series was computed, and the signature of the Hopf bifurcation was the development of a nonzero frequency component. For each run, V_c was measured before and after the experiment to determine the drift in V_c. The drift was a relatively constant 0.018 volts per h, which corresponds to a shift in ϵ of 0.003 per hour. This level of drift in conductivity did not adversely affect our ability to make comparison with theory and was accounted for in all values of ϵ that are reported here.

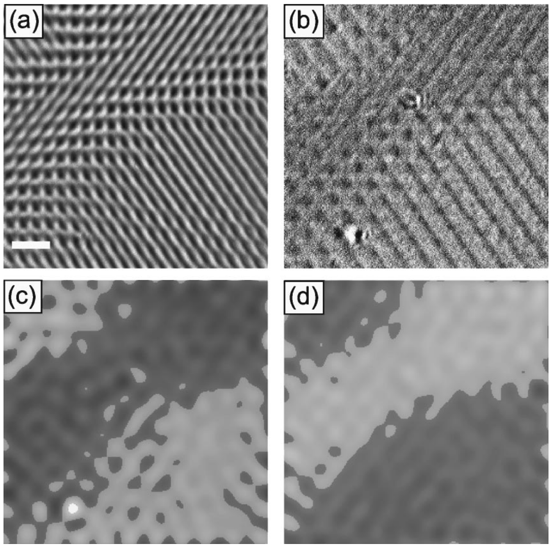

FIG. 2. Four images of the oblique roll state in a 0.7 mm $\times$0.7 mm region of the cell. The white bar in image (a) represents 0.1 mm. Images (a) and (b) are unprocessed. Images (c) and (d) have been processed with a low-pass Fourier filter to highlight the effects of the homogeneous twist of the director. The orientations of the $\lambda/4$ plate and the polarizers are as follows. (a) Unfiltered image with the polarizer aligned parallel to the undistorted director. (b) and (c) Unfiltered and filtered images, respectively, with the polarizer aligned perpendicular to the undistorted director. (d) Filtered image with the polarizer aligned perpendicular to the undistorted director and the $\lambda/4$ plate rotated 90° relative to the orientation used to take image (b).

III. EXPERIMENTAL RESULTS

Figure 2 shows four images of a typical pattern in the oblique roll regime, and Fig. 3 shows four images of a typical pattern above the bimodal varicose transition. For each figure, the images are all of the same pattern and the following protocols were used to take the images. Image (a) has the polarizer and analyzer parallel to each other and the undistorted director [setup shown in Fig. 1(a)]. The $\lambda/4$ plate is orientated at $+45°$ with respect to the undistorted director. In this case, one observes the usual shadow graph image. There is also an overall modulation of the intensity due to the homogeneous twist mode. For images (b), (c), and (d), the polarizer has been rotated 90° with respect to the undistorted director [setup shown in Fig. 1(b)]. Image (c) is a Fourier filtered version of image (b). A low-pass Fourier filter was used to highlight the intensity variation due to the homoge-

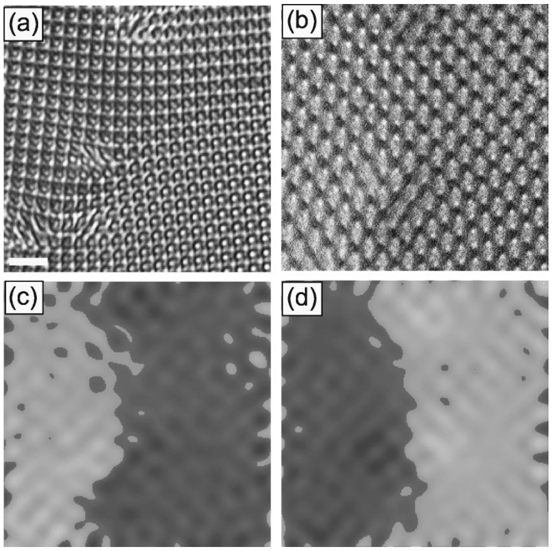

FIG. 3. Four images of the bimodal varicose state in a 0.7 mm $\times 0.7$ mm region of the cell. The white bar in image (a) represents 0.1 mm. Images (a) and (b) are unprocessed. Images (c) and (d) have been processed with a low-pass Fourier filter to highlight the effects of the homogeneous twist of the director. The orientations of the $\lambda/4$ plate and the polarizers are as follows. (a) Unfiltered image with the polarizer aligned parallel to the undistorted director. (b) and (c) Unfiltered and filtered images, respectively, with the polarizer aligned perpendicular to the undistorted director. (d) Filtered image with the polarizer aligned perpendicular to the undistorted director and the $\lambda/4$ plate rotated 90° relative to the orientation used to take image (b).

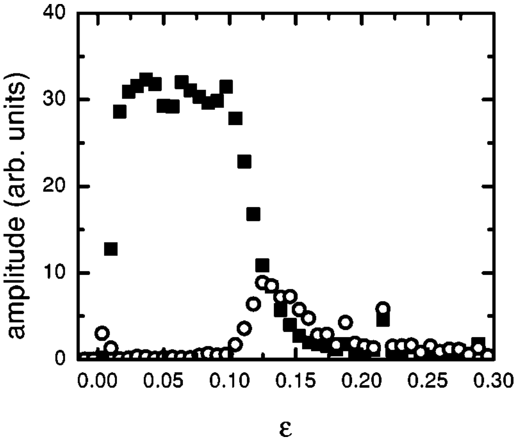

FIG. 4. Amplitude of the pattern at the fundamental wave vector **q** (solid squares) and at the dual wave vector **k** (open circles) at an angle of 85.3° with respect to **q**. This shows the bifurcation to oblique rolls at $\epsilon=0.007$ and the bimodal varicose instability at $\epsilon=0.1$. The initial small amplitude at **k** is due to the initial Hopf bifurcation for which zig and zag coexist. Within the resolution of these measurements, the amplitude of the dual wave vector **k** grows continuously at the bimodal varicose instability. See the text and Fig. 5 for a discussion of the apparent decrease in the amplitude of both modes for large ϵ.

neous twist of the director. This long-wavelength variation is difficult to detect in the raw image because of the residual focusing effects from the x-z distortion of the director. For image (d), the optical axis of the $\lambda/4$ plate is orientated $-45°$ relative to the polarizer and the image is again Fourier filtered with a low-pass filter. Therefore, image (d) should be the complement of image (c).

Both sets of images were obtained by jumping the voltage from below V_c to a value in the middle of the range for each state. A jump was used to create a pattern with both the zig and zag orientations to illustrate the different orientations of the in-plane twist in a single image. When the voltage is stepped slowly, a single orientation of the rolls exists over large regions of the cell.

With the orientation used for images (b) and (c), the brighter regions correspond to regions of negative twist. Therefore, Fig. 2(b) and 2(c) confirm that the twist orientation is opposite the pattern wave vector, as expected [15]. For example, the region of zig rolls (**q** at $+\theta$) in the lower right corner appears brighter than the region of zag rolls (**q** at $-\theta$) diagonally across the middle. Also, Fig. 2(d) is clearly the complement of Fig. 2(c), providing additional evidence that the source of the variations is an in-plane twist of the director.

In Fig. 3, the bimodal varicose pattern is shown. This state corresponds to the state SO2 in Ref. [21]. In general, the bimodal varicose pattern is described by the superposition of two modes with different amplitude and wave vectors, where one of the wave vectors is of the zig type and the other is of the zag type. This can be written as $A\cos(\mathbf{q}\cdot\mathbf{x})+B\cos(\mathbf{k}\cdot\mathbf{x})$, where A and B are the two amplitudes of the modes. In general, the two wave vectors are such that the modes are not a degenerate zig and zag pair. In this case, there are two degenerate bimodal varicose states. One formed when the initial wave vector **q** is a zig state, and one formed when **q** is a zag state. The two degenerate states are shown in Fig. 3. The left half of the image consists of a pattern where the zig-type rolls were the initial state and zag-type rolls grew as a result of the instability. The right half of the image is the reverse case. In this case, the angle between **q** and **k** is 80°. It is this superposition of a zig-type and zag-type roll that identifies the SO2 state as the bimodal varicose state. Furthermore, Figs. 3(c) and 3(d) confirm that the direction of the homogeneous twist is still determined by the wave vector with the maximum amplitude. This provides strong evidence for the mechanisms described in Ref. [15] as the source of the bimodal instability. Further work is needed to make quantitative measurements of the change in the amplitude of the twist mode as a function of the growth of the **k** mode.

Because the SO2 state corresponds to the bimodal varicose state, measurements of the transition point (ϵ_{BV}) exist for some parameter values [21]. These values for ϵ_{BV} are in very rough agreement with calculations of the twist-mode model [27]; however, detailed measurements of the transition points have not been made. For example, in this system, it has not been determined if the transition to the bimodal varicose is forward or backward. In order to elucidate the nature of the transition, Fig. 4 shows the amplitude of the pattern at the wave vectors **q** and **k** as a function of ϵ for the sample at $T=45°\mathrm{C}$. The amplitude of the pattern at a given wave vector is calculated from the power spectrum for each image. For each wave vector, the power is computed by summing the power in a 3 x 3 square centered on the wave vector. The amplitude is the square root of the power. Figure

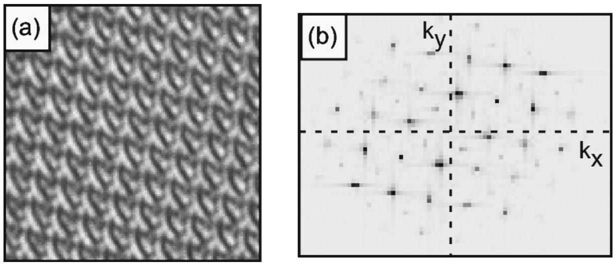

FIG. 5. (a) Image of the pattern at $\epsilon=0.15$. (b) Spatial power spectrum of the image shown in (a).

4 provides strong evidence that the bimodal varicose instability is forward, within the resolution of our measurements, because the amplitude of the **k** mode grows continuously from zero.

In Fig. 4, it appears that the amplitude of the **q** mode decreases at large ϵ. Though leveling off of the amplitude is expected, the decrease is most likely an artifact of optical nonlinearities that arise at high ϵ. This is demonstrated in Fig. 5, which shows a typical image of the bimodal varicose state at $\epsilon=0.15$. Also shown in Fig. 5 is the corresponding power spectrum. One clearly observes the large number of peaks corresponding to nonlinearities in either the optics or the pattern itself. In principle, one can compute the amplitude of the director variation A directly from the images. In electroconvection, the shadow graph images contain contributions proportional to both A and A^2. This adds some complication for calculating amplitudes of superimposed oblique rolls because the A^2 terms result in sums and differences of the two wave vectors. However, the real problem for this case is the additional nonlinearities that result in the plethora of diffraction peaks in Fig. 5(b). One such additional problem is the existence of caustics at these large amplitudes.

An additional feature of the electroconvection in the NLC I52 is that the initial bifurcation is actually a continuous, Hopf bifurcation to a state of superimposed zig and zag rolls. The large jump in amplitude to the pure zig state at $\epsilon=0.01$ corresponds to the transition from the initially traveling rolls to the stationary state. For all of the conductivities and temperatures reported on here, there was an initial Hopf bifurcation.

As ϵ is increased further, the bimodal varicose state experiences a Hopf bifurcation to the oscillating bimodal varicose state at $\epsilon\equiv\epsilon_H$. Figure 6 shows the power spectrum as a function of frequency for the wave vectors **q**, **k**, and for the zero wave vector of a typical time series above ϵ_H. The presence of a peak at finite ω is the signature of the oscillating bimodal state. These power spectra were computed by taking a time series of 64 images 0.5 s apart. The images covered a region containing approximately five wavelengths of the pattern. Each image was Fourier transformed, and a time series of the Fourier transforms at each wave vector of interest was constructed. Then, the power spectra of each of these time series was calculated. For these images, the arrangement of polarizer, $\lambda/4$ plate, and analyzer described in Fig. 1(a) was used. As discussed above, the use of image subtraction implies that the power in the zero wave vector corresponds to the amplitude of the twist mode, as it represents a long wavelength variation of the intensity. Also, for this state, the initial wave vector was of the zag-type and the dual wave vector was of the zig-type. Therefore, the direction of the twist is positive, and with the optical setup of Fig. 1(a), this produces an overall increase of the image intensity. Figure 6 illustrates two main points. First, the Hopf bifurcation corresponds to an oscillation of the roll amplitudes and the twist amplitude about their corresponding mean values (the large peak at zero frequency). Second, the oscillation amplitude is significantly less than the mean value.

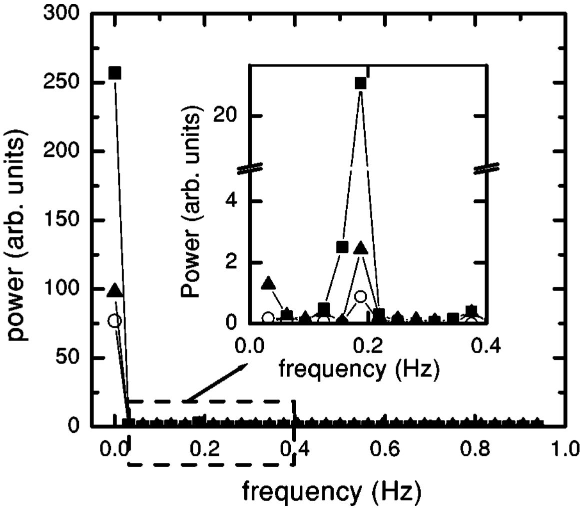

FIG. 6. Power spectra from a time series of images at three different wave vectors: zero wave vector (solid squares); **q** (solid triangles); and **k** (open circles). Here the initial wave vector **q** was of the zag type. The full power spectrum shows the large peak at zero frequency for each wave vector. This corresponds to the mean of each mode. The insert shows a close up view of the range indicated by the dashed box. The peak at approximately 0.2 Hz is the signature of the Hopf bifurcation from the bimodal varicose state.

The oscillating bimodal varicose, as defined in Ref. [22], is a pattern of the form $A(t)\cos(\mathbf{q}\cdot\mathbf{x})+B(t)\cos(\mathbf{k}\cdot\mathbf{x})$, where $A(t)$ and $B(t)$ oscillate roughly out-of-phase with each other and around different mean values. For the oscillating state observed here, Fig. 6 demonstrates that the mean values are different. Figure 7 illustrates the behavior of the oscillating bimodal varicose in real space and illustrates the out-of-phase nature of the oscillations. The image in Fig. 7 is one of the individual frames used to compute the power spectra shown in Fig. 6. Because of the optical nonlinearities, the

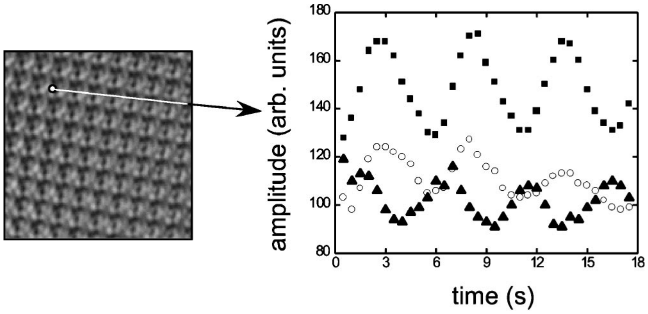

FIG. 7. Time series of the amplitude of the three modes whose power spectra are plotted in Fig. 6. The time series is the average amplitude of a region 2 pixels by 2 pixels that is shown in the image by the white dot. The three modes are identified by their wave vector: zero wave vector (squares), **q** (circles), and **k** (triangles).

easiest way to directly observe out-of-phase oscillations is to plot the local behavior of the pattern after Fourier filtering. This is shown in the plot in Fig. 7. The plot is constructed as follows. For each image in the time series, the Fourier transform is computed. Then, a Hanning window is applied to the region around the wave vector of interest (and its complex conjugate). The inverse Fourier transform of the result produces a real space image that corresponds to the mode of interest. In this real space image, the pixels in a 2×2 region are averaged. The region is shown by the dot in the image in Fig. 7. A time series of these average values is then constructed. The plot in Fig. 7 is subset of the longer time series used to compute the power spectra of Fig. 6.

Figure 7 clearly illustrates the oscillations of the twist-mode (squares), zig-type mode (triangles), and zag-type mode (circles) that comprise the oscillating bimodal varicose. The optical arrangement of Fig. 1(a) was used while taking this time series. Therefore, the positive amplitude of the twist-mode represents a positive rotation angle. This is consistent with the dominant mode being of the zag-type. Also, an increase in the zero wave vector intensity represents an increase in the twist-mode amplitude, which is correlated with the increase in the zag mode amplitude. A mechanism for the oscillating bimodal varicose is discussed in Ref. [15], and the evidence provided by Figs. 6 and 7 for this mechanism is discussed in Sec. IV.

IV. DISCUSSION

The results presented in this paper highlight three main points. First, the twist mode is present in the oblique roll states in the NLC I52, as it should be. Because it is a weakly damped mode [15], its amplitude is actually relatively large. Therefore, it must be included in any extended weakly nonlinear description of the system.

Second, the observed qualitative features of the oscillating bimodal state are consistent with the mechanism proposed in Ref. [15]. In particular, the results presented in Fig. 7 provide strong evidence that the twist mode is responsible for the dynamics of this state. The plot in Fig. 7 should be compared to the analogous plot in Fig. 8 of Ref. [15]. In both cases, the amplitudes of the zig and zag-type rolls are out-of-phase with each other. The twist-mode is found to oscillate with a phase intermediate to the two modes. This is strong evidence for the proposed director-wave-vector frustration mechanism where the oscillations of the twist mode mediate the oscillations in the **q** and **k** modes [15].

Finally, the WEM effects may remain important in the nonlinear states and have an effect on the location of the bimodal varicose transition and the following Hopf bifurcation. The fact that the WEM effects are present is clearly shown by the initial Hopf bifurcation that is present at all the parameters used here. The calculations in Ref. [15] that include the twist amplitudes are based on the standard model of electroconvection, which do not allow for the observed primary Hopf bifurcation. However, the fact that the traveling waves were always replaced with a stationary pattern at $\epsilon\leqslant0.01$ suggests that the WEM effects are ''weak'' in some sense. Therefore, it is not unreasonable to qualitatively compare the results presented here with calculations based on the twist-mode model. However, as is shown in Table I, there is some quantitative disagreement between the twist-mode model and the experiment.

TABLE I. Comparison of theoretical and experimental values for two different temperatures.

Temperature (°C)	θ	α	ϵ_{BV}	ϵ_H
42 (exp.)	32.0°	82.4°	0.079	0.17
42 (theory)	32.0°	82°	0.08 [a]	none
55 (exp.)	37.9°	86.3°	0.03	0.19
55 (theory)	37°	80°	0.06	none

[a] A maximum in the growth rate of the dual is found, but the growth rate is still negative.

Table I shows a comparison between calculations [27] and experiment for two temperatures for the following measured quantities: the initial angle of the rolls with respect to the undeformed director (θ); the angle α between **q** and **k** at the bimodal varicose instability; the transition point to the bimodal varicose state (ϵ_{BV}); and the subsequent Hopf bifurcation to the oscillating bimodal varicose (ϵ_H). There is good agreement between θ and α. The agreement for θ is not surprising because the WEM predicts only a small shift in θ from the standard model value. Likewise, the agreement for α is not surprising because the WEM does not appear to shift angles significantly. The asterisk next to the calculated value of ϵ_{BV} for the $T=42\,^{\circ}\mathrm{C}$ case indicates that there is a maximum in the growth rate of **k** at this point, but the growth rate is still negative. In fact, for this temperature, the growth rate of **k** does not become positive within the twist-mode model. Also, for the $T=55\,^{\circ}\mathrm{C}$ case, the calculation predicts a value for ϵ_{BV} that is too large. For all the parameter values used in the experiment, a transition to the oscillating bimodal varicose from the bimodal varicose state was observed. Over this same range of parameters, the calculations predict a restabilization of a single roll state that supersedes the oscillating bimodal varicose.

In addition to possible WEM effects, there are a number of additional sources for the above outlined quantitative disagreements between experiment and the twist-mode model. First, the locations of ϵ_{BV} and ϵ_H have not yet been calculated in a fully nonlinear calculation and can only be estimated within the context of the extended weakly nonlinear analysis. Second, there are issues of pattern selection that are not addressed in the weakly nonlinear analysis. For example, even though the weakly nonlinear analysis predicts the restabilization of the oblique rolls, the pattern may still select the oscillating bimodal varicose state. Finally, there remains important uncertainties in the material parameters of the NLC I52 that make quantitative comparison between theory and experiment difficult.

The confirmation of the existence of the twist mode in electroconvection in the NLC I52 has important consequences for both the states of spatiotemporal chaos [18] and the localized worm states [19] that have been observed in this system. Because both of these states involve the superposition of oblique rolls, the twist mode must automatically be present, as observed here. In principle, if the states were a superposition of equal amplitudes of zig and zag, the twist mode would have zero amplitude as the two set of rolls produce opposite twists. However, for the state of spatiotemporal chaos, the amplitudes vary irregularly. Therefore, the twist mode may play an active roll in the dynamics as a mediator between the zig and zag rolls. Likewise, in the worm state, the zig and zag rolls have different amplitudes at the edges of the worm. Therefore, the twist mode may play a role in the localization mechanism of the worms as an additional slow field.

ACKNOWLEDGMENTS

I thank Emmanuel Plaut and Werner Pesch for useful discussions Also, I thank Emmanuel Plaut for providing me with unpublished theoretical calculations. This work was supported by NSF Grant No. DMR-9975479.

[1] For reviews of pattern formation, see M. C. Cross and P. C. Hohenberg, Rev. Mod. Phys. **65**, 851 (1993); J. P. Gollub and J. S. Langer, *ibid.* **71**, s396 (1999).

[2] For a recent review of pattern formation in liquid crystals, see A. Buka and L. Kramer, *Pattern Formation in Liquid Crystals* (Springer-Verlag, New York, 1996).

[3] Review articles on electroconvection can be found in I. Rehberg, B. L. Winkler, M. de la Torre Juárez, S. Rasenat, and W. Schöpf, Festkoerperprobleme **29**, 35 (1989); S. Kai and W. Zimmermann, Prog. Theor. Phys. Suppl. **99**, 458 (1989); L. Kramer and W. Pesch, Annu. Rev. Fluid Mech. **27**, 515 (1995).

[4] P. G. de Gennes, *The Physics of Liquid Crystals* (Claredon Press, Oxford, 1974); S. Chandrasekhar, *Liquid Crystals* (Cambridge University Press, Cambridge, England, 1992).

[5] R. P. Twitchell and E. F. Carr, J. Chem. Phys. **46**, 2765 (1967).

[6] W. Helfrich, J. Chem. Phys. **51**, 4092 (1969).

[7] E. Bodenschatz, W. Zimmermann, and L. Kramer, J. Phys. (France) **49**, 1875 (1988); L. Kramer, E. Bodenschatz, W. Pesch, W. Thom, and W. Zimmermann, Liq. Cryst. **5**, 699 (1989).

[8] W. Zimmermann, in *Nematics: Mathematical and Physical Aspects*, edited by J.-M. Coron, J. M. Ghidaglia, and F. Helein, Vol. 332 of NATO *Advanced Studies Institute Series C: Mathematical & Physical Sciences* (Kluwer, Dordrecht, 1991), p. 401.

[9] I. Rehberg, S. Rasenat, J. Fineberg, M. de la Torre Juárez, and V. Steinberg, Phys. Rev. Lett. **61**, 2449 (1988).

[10] I. Rehberg, S. Rasenat, and V. Steinberg, Phys. Rev. Lett. **62**, 756 (1989).

[11] E. Plaut, W. Decker, A. G. Rossberg, L. Kramer, W. Pesch, A. Belaidi, and R. Ribotta, Phys. Rev. Lett. **79**, 2367 (1997).

[12] S. Rudroff, H. Zhao, L. Kramer, and I. Rehberg, Phys. Rev. Lett. **81**, 5144 (1998).

[13] M. Treiber and L. Kramer, Mol. Cryst. Liq. Cryst. **261**, 311 (1995).

[14] M. Dennin, M. Treiber, L. Kramer, G. Ahlers, and D. S. Cannell, Phys. Rev. Lett. **76**, 319 (1996).

[15] E. Plaut and W. Pesch, Phys. Rev. E **59**, 1747 (1999).

[16] E. Plaut and R. Ribotta, Eur. Phys. J. B **5**, 265 (1998).

[17] M. Dennin, Ph.D. thesis, Department of Physics, University of California at Santa Barbara, 1995 (unpublished).

[18] M. Dennin, G. Ahlers, and D. S. Cannell, Science **272**, 388 (1996).

[19] M. Dennin, G. Ahlers, and D. S. Cannell, Phys. Rev. Lett. **77**, 2475 (1996).

[20] M. Treiber and L. Kramer, Phys. Rev. E **58**, 1973 (1998).

[21] M. Dennin, D. S. Cannell, and G. Ahlers, Phys. Rev. E **57**, 638 (1998).

[22] E. Plaut, L. Pastur, and R. Ribotta, Eur. Phys. J. B **5**, 283 (1998).

[23] U. Finkenzeller, T. Geelhaar, G. Weber, and L. Pohl, Liq. Cryst. **5**, 313 (1989).

[24] E.H.C. CO., Ltd., 1164 Hino, Hino-shi, Tokyo, Japan.

[25] S. Rasenat, G. Hartung, B. L. Winkler, and I. Rehberg, Exp. Fluids **7**, 412 (1989).

[26] H. Amm, R. Stannarius, and A. G. Rossberg, Physica D **126**, 171 (1999).

[27] E. Plaut (private communication).